Proceedings of ASME Turbo Expo 2011
GT2011
June 6-10, 2011, Vancouver, British Columbia, Canada

GT2011-45737

THE INFLUENCE OF INLET CONTRACTION ON VANE AERODYNAMIC LOSSES AND SECONDARY FLOWS WITH VARIABLE TURBULENCE AND REYNOLDS NUMBER

N.H.K Chowdhury, P.K. Dey, and F.E. Ames
Mechanical Engineering Dept.
University of North Dakota

ABSTRACT

Exit survey measurements comparing exit losses for a constant inlet height cascade and a contracting inlet cascade have been acquired in a low speed wind tunnel facility. The measurements were taken for both a low and a high turbulence level across a four to one range in chord Reynolds number (500,000, 1,000,000, and 2,000,000). The high intensity turbulence has been generated using a simulated aero-combustor for both cascades. Exit survey measurements have been acquired for the two cascades using a five-hole cone probe at stations representing an exit location of ¼ axial chord downstream from the trailing edge plane. Measurements detail total pressure loss, turning angle, and secondary velocities. At the low turbulence condition, the contracting inlet cascade shows a significant reduction in losses compared with the constant height inlet cascade. The contracting inlet cascade also features an aft loaded vane profile which may have some impact on the development of secondary flows. The constant cross-section cascade uses a fully loaded vane profile. The difference in losses between the two cascades is also significant at the high turbulence condition. However, at the high turbulence condition, the losses for the contracting inlet cascade are greater than the constant cross-section cascade. These increased losses are believed to be due to the more aggressive turbulence of the contracting inlet case. The contracting inlet effectively moves the vane leading edge plane forward into the exit of the combustor where the vane passage is subjected to more aggressive turbulence levels.

INTRODUCTION

First vanes often have contracting flow paths as they transition from combustion system to the first stage rotor. This contraction has the potential to improve turbine aerodynamics by reducing the impact of some of the secondary flows in turbine passages. The present paper studies the influence of inlet contraction on turbine vane aerodynamic losses. The baseline linear cascade in this study has a constant height inlet while the second cascade has a contracting inlet which maximizes the acceleration at the leading edge to reduce the impact of leading edge vortex system on aerodynamic losses. The two cascades have similar spans, spacing, and turning. Measurements are acquired in the same facility at both low and aero-combustor turbulence levels over a four to one range in Reynolds number. Previously, vane midline heat transfer was investigated in the two cascades [1, 2]. Additionally, vane endwall heat transfer was documented for the baseline cascade [3]. The present measurements provide a basis to assess the influence of inlet contraction on aerodynamic losses at both low and engine relevant turbulence conditions.

BACKGROUND

Understanding and minimizing turbine aerodynamic losses is critical to the design of high performance gas turbine engines. Denton [4] reviews loss mechanisms in turbomachinery and suggests that turbine passage losses can include profile losses, endwall losses, and leakage losses. Glassman [5] attributed the primary origin of profile losses to airfoil boundary layer development and trailing edge losses. Denton suggests that turbulent mixing across inertial velocity gradients outside of boundary layers and wakes can also contribute to turbine losses. Denton indicates that endwall losses can account for as much as 1/3 of the total passage loss. Moore et al. [6] found that a significant level of losses, up to 1/3, occurs downstream from the trailing edge due to deformation work. Gregory-Smith and Cleak [7] studied the influence of grid turbulence (Tu = 5%) on aerodynamic losses finding a 7% increase in profile losses yet at the same time finding a 12% decrease in endwall losses. Ames and Plesniak [8] investigated the influence of simulated aero-combustor turbulence on profile losses and wake growth in a linear cascade. They were able to attribute wake losses to vane boundary layer growth and trailing edge separation loss. They also found a "background" total pressure loss outside of the normal wake for the high turbulence cases. They suggested that a majority of this loss was a result of redistribution of wake and endwall losses due to turbulent diffusion. However they estimated that at least 1/3 of this "background" loss was due to turbulent mixing within the passages. Sieverding [9] reviewed secondary flows in turbine passages presenting the models of Klein [10] and Langston et al. [11]. Langston's model included both the pressure and suction side legs of the horseshoe vortex and the passage vortex. Sieverding [9] suggested that the corner vortex is the result of the interaction of the passage vortex with the suction surface. Marchal and Sieverding [12] found secondary losses increased downstream

from the maximum velocity. Endwall contouring and leading edge fillets have been approaches used to reduce secondary losses in turbine passages. Burd and Simon [13] studied flow in a cascade with one sided endwall contouring. They found that the endwall contouring produced an acceleration which reduced the size and strength of secondary flow features showing a much larger influence near the contoured endwall. Zess and Thole [14] investigated a leading edge fillet on secondary losses finding reduced turbulent kinetic energy levels in the endwall region due to the elimination of the unsteady horseshoe vortex. Becz et al. [15, 16] studied fillet and bulb leading edge modifications and found loss reductions with the fillet and higher turning with the bulb. Ingram et al. [17] reduced the cross-passage pressure gradient using endwall profiling and found a 24% reduction in secondary losses. The present investigation compares a conventional linear cascade with a constant span inlet with a similar cascade with a contracting inlet. The inlet contraction maximizes the acceleration at the leading edge to reduce the impact of inlet separation including leading edge vortex system on aerodynamic losses. The aft loaded vane is designed to reduce profile losses by delaying suction surface transition and moving the maximum velocity location downstream in the passage, impeding the growth of secondary losses.

NOMENCLATURE

beta	turning angle, (°), also β
C	vane true chord length, m
Cp	Specific heat at constant pressure, J/kg/K
h	heat transfer coefficient, $W/m^2/K$
Lu	energy scale, $Lu = 1.5 \|u'\|^3/\varepsilon$
Lx	longitudinal integral scale of u' fluctuation
Omega	total pressure loss coefficient, $[P_{T,IN}-P_{T,EX}]/[P_{T,IN}-P_{S,EX}]$, also Ω
P	Pressure, Pa
Re_C	Reynolds number based on true chord and exit conditions
S	vane surface arc length measured from stagnation point, m
St	Stanton number, $h/\rho U_\infty Cp$
T	temperature, K
Tu	turbulence level, $Tu = \|u'\|/U_\infty$
U_∞	freestream velocity, m/s
u', |u'|	streamwise component rms fluctuation velocity, m/s

Greek Letter Symbols

β	turning angle, (°), also beta
ε	turbulent dissipation rate, m^2/s^3
ν	kinematic viscosity, m^2/s
ρ	fluid density, mass per unit of volume, kg/m^3
Ω	total pressure loss coefficient, $[P_{T,IN}-P_{T,EX}]/[P_{T,IN}-P_{S,EX}]$, also Omega

Subscripts

EX	refers to conditions at the nozzle exit plane
IN	refers to conditions at the nozzle inlet plane
S	refers to static condition
T	refers to total or stagnation condition
∞	evaluated in the free stream

EXPERIMENTAL APPROACH

Exit survey measurements were acquired in both constant height and contracting inlet cascade test sections in a low speed wind tunnel facility. The contracting inlet cascade has a 30 degree inlet on both endwalls into the leading edge plane of the vanes. This inlet contraction can be seen in **Figure 1**, which provides a schematic for the mock aero-derivative combustor turbulence generator. The 30 degree contraction ends at the vane leading edge plane and transitions through a 10.16 cm radius 30 degree arc into the constant section portion of the cascade. Pushing the first stage vane forward into the contracting portion of the combustor nozzle places the leading edge plane 32 cm forward of the vane location for the original constant height cascade. The leading edge of the vane is now located in a lower velocity but more highly turbulent flow when compared to the constant height cascade. The inlet flow accelerates toward the vane leading edge plan to help reduce the impact of the vane horseshoe vortex and passage vortex systems. The nozzle system for the low turbulence condition has a similar inlet contraction compared with the aero-combustor turbulence generator shown in **Figure 1**.

Wind Tunnel and Cascade Test Section. The large scale low speed cascade wind tunnel facility is pictured in **Figure 2**. The facility uses a 45 kW blower which entrains air through a large industrial filter system to remove particulates. The variable frequency controlled blower can move 6.6 m^3/s of air at a static pressure rise of 5000 Pa. Air discharging from the blower passes through two multivane diffusers before entering a heat exchanger used to keep the tunnel air temperature constant during heat transfer measurements. The air then moves into a screen box before accelerating through a 3.6 to 1 contraction nozzle. The nozzle directs the air into the cascade test section. A two axis traversing section which positions a 5-hole cone probe sits at the exit of the cascade. The air passing through the traversing section enters a multivane diffuser to extend the Reynolds number range of the tunnel. An oblique header is attached to the diffuser to direct the airflow away from light fixtures in the ceiling.

The constant height cascade section attaches to the nozzle after the 3.6 to 1 area ratio contraction for the low turbulence configuration shown in **Figure 2**. The aero-combustor turbulence condition is developed by replacing the nozzle with a mock aero-derivative combustor similar to the one shown schematically in **Figure 1**. However, the aero-combustor for the constant height cascade section completes its 2 to 1 area ratio contraction before the cascade test section.

The contracting inlet cascade shown in **Figure 3** attaches to the nozzle at a 30 degree angle from both endwalls and 12.7cm upstream from the vane leading edge plane. The aero-combustor used with the contracting inlet cascade is built to fit to the inlet of the contracting endwall cascade. Access ports for inlet total pressure, total temperature, and hot wire measurements are located 7 cm upstream from the vane leading edge plane. The cascade has upper and lower bleed flow adjustments above the upper vane and below the lower vane along calculated streamlines. A row of inlet static pressure taps, 7.6 cm upstream from the leading edge plane, is used to monitor inlet flow uniformity. The cascade has flexible tailboards starting from the trailing edges of the upper and lower vanes. A row of exit static pressure taps located ¼ axial chord downstream from the trailing edge plane is used to monitor exit periodicity as well as to monitor the exit condition. The four vane three passage cascade uses an aft loaded vane design to help reduce aerodynamic losses by delaying transition on the suction surface.

Vane Design Comparison. The aft loaded vane design is shown in **Figure 4** and compared to the conventional vane profile used on the constant inlet height cascade. The geometries of the aft loaded and conventional or forwarded loaded vanes are compared in **Table 1.**

The aft loaded vane pressure distribution is compared with the fully loaded profile of the conventional vane in **Figure 5**. These profiles have been designed to simulate vane pressure loadings at high subsonic Mach numbers. Midline pressure distributions were acquired experimentally using a foam vane with a mold cast epoxy outer surface which incorporated 40 surface static pressure taps drilled at

midspan of the cascade. The pressure vane, used for aerodynamic testing, can be inserted into a vane shaped window into the third vane position from the bottom. The experimental pressure distribution for the aft loaded vane is compared with a 3D circumferentially periodic FLUENT [18] calculation. The pressure distribution for the conventional vane compared with a 2D periodic FLUENT calculation. The 3D FLUENT calculation was needed to account for the acceleration due to the contracting inlet. Both experimental pressure distributions were acquired at chord exit Reynolds numbers of 2,000,000 based on exit conditions. The figure plots local static to inlet total pressure ratio as a function of surface distance. Negative distance is determined along the pressure surface while positive distance starts at the stagnation line along the suction surface. The conventional vane accelerates quickly and peaks early along the suction surface showing a typical fully loaded profile. The aft loaded vane shows slightly more gradual acceleration on the suction surface and peaks after mid arc along the suction surface. The aft loading of the vane is expected to move the location of transition further downstream producing a slightly lower level of profile loss. However, the vane also requires a greater level of diffusion in the aft portion of the vane. Generally, the experimental pressure distributions are very consistent with the FLUENT predictions providing confidence in the midspan aerodynamics set up by the cascades.

Inlet Turbulence Conditions. The inlet turbulence conditions documented for the contracting inlet and constant height cascades are documented in Table 2. The inlet velocities are different for the two cascades as the measurement location for the contracting inlet is located in the contraction unlike the constant height cascade. The inlet turbulence conditions for the constant height cascade were measured at 5 evenly spaced circumferential locations over 3 spanwise positions 7 cm upstream of the vane inlet plane and then averaged. Generally, the low turbulence condition produces a 0.7% turbulence level with an inlet velocity which averages 33% higher than the contracting inlet cascade. The aero-combustor turbulence generator produces a turbulence intensity of around 14% with an energy scale of about 7 cm. Inlet velocities for the aero-combustor cases average 13% higher than for the contracting inlet. The turbulence conditions for the contracting inlet are measured at 5 evenly spaced circumferential locations over 3 spanwise positions 7 cm from the leading edge plane of the vane and averaged. The inlet turbulence level averages 1.0% for the low turbulence inlet. However, the velocity of the flow is noticeably lower than constant section inlet. The turbulence levels for the aero-combustor case average nearly 21% due to the close proximity to the aero-combustor as well as due to the slightly lower inlet velocities. The upstream location of the contracting inlet cascade makes the turbulence condition significantly more aggressive. The measured turbulent dissipation levels are approximately 2.8 times the levels measured for the constant height cascade. Note that turbulent dissipation rates were determined from a line fit to the inertial subrange of the measured u' spectrum.

Exit Surveys. Exit survey measurements were acquired in two linear cascades in a plane which was nominally perpendicular to the flow and 21 cm downstream from the vane trailing edge. Exit survey measurements included total pressure loss, turning angle, and secondary velocities. Measurements were acquired using a 4.76 mm diameter 5-hole cone probe with a 60° included angle. The probe was calibrated at the velocities for the three exit Reynolds numbers over an angle range of +/- 25° for both pitch and yaw. Measurements at the 2,000,000 chord exit Reynolds number were acquire using 5 miniature differential piezoresistive pressure sensors with a full scale range of 5000 Pa. Measurements at 500,000 and 1,000,000 Reynolds numbers were acquired using sensors with a full scale range of 1250 Pa. The four ports on the probe were measured referenced to the center port and the difference between the inlet total pressure and the cone centerline pressure was also acquired. The pressure lines between the probe and sensor were damped to reduce averaging requirements for resolved statistics. Each pressure used for the survey was averaged between 25 and 75 times depending on the turbulence level and the Reynolds number. Measurements in the cross passage direction were acquired from midpassage between vanes two and three to midpassage between vanes three and four at 25 positions over 11.67 cm. The traverse in the span direction began at with the probe at a location 0.476 cm off the endwall and finished at midspan using a total of 27 positions.

Data Acquisition. Inlet total, inlet and exit static pressures as well as vane surface static pressure were acquired using a custom pressure scanner. The scanner incorporates two Rosemount pressure transmitters run in parallel with full scale ranges of 250 Pa and 5000 Pa with 0.1% of scale accuracy. The most sensitive transmitter in range is selected for each reading which is averaged 20 times for each measurement. Inlet total temperatures are acquired using type K fine wire thermocouples connected to an HP3497A data acquisition unit through a passive constant temperature reference box. A thermocouple in an ice bath is used to reference the passive junction box. The HP3497A has an integral digital voltmeter with 1 μV sensitivity. The Allsensor piezoresistive pressure sensors are powered using a 5 VDC Acopian power supply and are read with the HP3497A. HP3497A also is used to read the Rosemount pressure transmitters.

Uncertainty Analysis. Measurement uncertainties were estimated using the root sum square method described by Moffat [19]. Uncertainty estimates were determined for normalized vane surface pressure, total pressure loss, Ω, and turning angle, β. The uncertainty in the reported pressure ratio, P_S/P_T, was estimated to be +/- 0.0005 due to both uncertainties in the pressure measurement and uncertainties in position. The uncertainty in total pressure loss was estimated to be as high as 0.01 for the high turbulence condition and 0.008 for the low turbulence condition at the lowest Reynolds number. This significant uncertainty is due to bias error in the readings at this Reynolds number when using the 1250 Pa sensors. The bias error in Ω for the 500,000 Reynolds number is about 0.007 compared with a bias error for Ω of 0.0018 for the 1,000,000 and 2,000,000 Reynolds number cases. Consequently, the uncertainty in total pressure loss, Ω, was found to be much lower (+/- 0.002 to +/-0.0025) for the two higher Reynolds numbers. The uncertainty in the reported angle is due to bias error, unsteadiness, and setup error. The estimated uncertainty in exit angle due to bias error is estimated to be +/- 0.26° while the uncertainty in angle due to unsteadiness is estimated to be +/- 0.25°. The estimated uncertainty in angle due to set up is estimated to be +/- 0.20°. The setup of the exit survey probe did not change between high and low turbulence condition. However, the exit survey mechanism did change between the two cascades. Uncertainty in the single wire measurement of turbulence intensity is estimated to be +/- 3% of the reported value. Uncertainty in determining turbulent scale is estimated to be 11%. All uncertainties have been reported at 95% confidence intervals.

EXPERIMENTAL RESULTS

The focus of this paper is to compare the aerodynamic losses of a conventional cascade with a constant height inlet to a cascade with a contracting inlet. The cascades were run at both a low and an aero-combustor turbulence condition. Additionally, each cascade was run at Reynolds numbers of 500,000, 1,000,000, and 2,000,000 based on true chord and exit condition. The contracting inlet of the cascade required the inlet of the cascade to be integrated into the nozzle used

for both the low and the aero-combustor flow conditions. The impact of this integration into the nozzle was not significant for the low turbulence condition. However, for the aero-combustor turbulence conditions this integration effectively moved the cascade closer to the turbulence generator by 32 cm which caused the turbulence to be significantly more aggressive. This section compares the total pressure loss contours along with their secondary velocity vectors for the two cascades at the two turbulence conditions. This section also compares circumferentially averaged total pressure loss and angle distributions for the two cascades at the two inlet turbulence levels and for the contracting inlet cascade as a function of Reynolds number. Finally, the passage averaged loss values are compared as a function of Reynolds number for the two cascades at the two inlet turbulence conditions.

Boundary Layer Heat Transfer Distributions. Profile losses are known to consist of boundary layer momentum losses and trailing edge separation losses. Consequently, vane boundary layer development and trailing edge thickness significantly influence the magnitude of profile losses. The present measurements use a conventional vane and an aft loaded vane with the same surface distance and the same trailing edge thickness. Heat transfer distributions are very useful in understanding the state of the boundary layer with flow over a surface. Vane surface Stanton number distributions are presented in **Figure 6** (see references [1, 2]) for flow over both the conventional (solid symbols) and aft loaded (open symbols) vanes for both low and aero-combustor turbulence for an exit chord Reynolds number of 1,000,000. The heat transfer levels for the low turbulence (LT) condition shown with the square symbols are very similar except in the stagnation region. The lower inlet velocity of the contracting inlet to the cascade lowers the heat transfer level in the leading edge region. On the pressure surface (negative distance) the heat transfer levels are very similar. On the suction surface (positive distance) heat transfer levels for the aft loaded vane are slightly lower until the adverse pressure gradient near the trailing edge causes the start of transition. The heat transfer levels for the aero-combustor (AC) turbulence are presented with diamond symbols and show slightly higher heat transfer levels for the contracting inlet cascade except near the stagnation region where velocities are lower. The contracting inlet cascade is integrated into the nozzle of the aero-combustor which brings the cascade leading edge plane 32 cm closer to the combustor. **Table 2** shows substantially higher turbulence conditions for the contracting inlet cascade for the aero-combustor condition. These more aggressive turbulence conditions are indicated by the higher Stanton numbers on the pressure surface as well as the earlier transition and the higher heat transfer levels on the suction surface. The slightly higher Stanton numbers for the contracting inlet cascade for the aero-combustor condition also suggest slightly higher profile losses.

Exit Loss Contours Low Turbulence. The exit surveys using the five-hole cone probe produced an exit plane view of total pressure loss contours and secondary velocities. Total pressure loss contours Ω (Omega) for the constant height inlet cascade at the low turbulence condition are shown in **Figure 7** for an exit Reynolds number of 1,000,000. Generally, each contour line represents an increment of 0.025 in the total pressure loss. The contours show a relatively thin and nearly two-dimensional wake at mid span due to the laminar flow on the vane surface. The contours also evidence a significant secondary loss core. The secondary loss core has been convected about 4.3 cm or 17% of span off the endwall suggesting a relatively strong passage vortex. The secondary velocity vectors show the secondary loss core is actively being convected off the endwall and away from the suction surface. This movement away for the suction surface results in under turning in this region. The loss along the endwall indicates a relatively thin endwall boundary layer which is very consistent with the relatively modest level of under turning. A high loss region is located at the center of the wake near the endwall which is evidence of a corner vortex, believed to be the result of the interaction of the passage vortex with the suction surface. The mass averaged passage loss for this condition was determined to be 0.0366 while the profile loss was determined to be 0.0240 near midspan. The low turbulence condition results in a very low level of profile and passage losses which are tabulated for all the conditions in **Table 3**.

Total pressure loss contours for the contracting inlet cascade at the low turbulence condition are shown in **Figure 8** for an exit Reynolds number of 1,000,000. The wake in the central span of the passage is very thin and two dimensional due to the laminar boundary layers developing on the vane. The wake is somewhat thinner but slightly deeper than the constant height cascade. The secondary loss core for the contracting inlet cascade is similar to the loss core for the constant height inlet cascade but has a lower position off the endwall. The center of the loss core is about 3.8 cm or 15% of span off the endwall suggesting a somewhat weaker passage vortex. The contracting inlet on the cascade is expected to weaken the strength of the horseshoe vortex system and thin the boundary layer entering the vane passage. These two effects would be expected to reduce the low momentum fluid adjacent to the endwall and thereby reduce the strength of the passage vortex. The loss contours for the contracting inlet cascade also show mild overturning near the endwall as well as evidence of a corner vortex. The mass averaged loss for this condition was determined to be 0.0311 which is a 0.0055 reduction in total pressure loss between the straight and contracting inlets. Considering the bias error in the measurement is on the order of 0.002 this difference is considered significant.

Endwall Loss Contours Aero-combustor. The character of total pressure loss contours and secondary velocity vectors is much different for the aero-combustor condition. Total pressure loss contours and secondary velocity vectors are presented in **Figure 9** for the aero-combustor condition for the constant height inlet cascade. The midspan wake is broad and two-dimensional due to both the increased skin friction caused by early transition on the suction surface as well as additional turbulent augmentation of boundary layer skin friction. The breadth of the wake is due to the action of the large scale turbulence promoting mixing across the developing boundary layers and wake. The action of the large scale turbulence can also produce an unsteadiness which tends to show a more dissipated distribution in the time averaged view of the five-hole cone probe measurements. The passage vortex is barely present indicating the combined mixing action and unsteadiness of the turbulence has obscured evidence of its existence in a time averaged sense. Total pressure losses and significant overturning along the endwall are clearly present. The mid wake peak in losses at the endwall along with the vorticity there is evidence of a significant corner vortex. The mass averaged loss across the passage was determined to be 0.0567 for this condition or 0.02 more than the low turbulence condition for this cascade. This incremental increase in total pressure loss is due to early transition and skin friction augmentation on the vane and endwall surfaces caused by the high intensity turbulence. A portion of the incremental loss can be attributed to the inlet boundary layer (Ames et al. [20]) for this condition. Additionally, Ames and Plesniak [8] suggest a portion of this loss increase can be attributed to the action of the high intensity large scale turbulence working on inertial velocity gradients in the flow. At this high turbulence level, a significant level of total pressure loss is measured outside of the normal extent of the wakes and a portion of this "background" loss is attributed to turbulent mixing

action outside the normal viscous shear layers in the flow. However, the difference between the passage averaged loss and profile loss are less for this high turbulence condition as compared with the low turbulence condition. This reduction of endwall losses due to enhanced turbulent mixing has been previously noted by Gregory-Smith and Cleak [7] and is attributed to reduced separation losses on the endwall in the presence of elevated turbulence levels.

The total pressure loss contours for the contracting inlet cascade are presented in **Figure 10** for the aero-combustor turbulence condition at a chord Reynolds number of 1,000,000. The general character of the loss contours for the contracting inlet cascade is very similar to the constant height inlet cascade for this aero-combustor turbulence condition. However, a few noticeable differences include a lack of any secondary loss core and a noticeably broader wake near the endwall. These differences are likely due to the enhanced turbulent mixing and unsteadiness caused by the more aggressive turbulence conditions of the contracting inlet cascade. The measured midspan loss difference between the constant height and contracting inlet cascades is within the uncertainty of the measurements. However, the passage averaged total pressure loss for the contracting inlet cascade is 0.0600 compared with a value of 0.0567 for the constant inlet cascade. This increase in loss with the contracting inlet cascade is significant and perhaps counter intuitive based on the results for the low turbulence condition. However, the action of the aero-combustor turbulence could be expected to eliminate much of the endwall separation loss and thus much of the advantage for the contracting inlet cascade. Also, the contracting inlet which effectively moves the cascade 32 cm forward toward the combustor results in a much more aggressive turbulence condition as documented in **Table 2**.

Cross-Passage Averaged Total Pressure Loss and Turning Angle. **Figure 11** compares the cross-passage averaged total pressure loss (Omega) as a function of span for the constant and contracting inlet cascades for the two turbulence conditions. The low turbulence loss profiles are very similar. Near midspan the constant height inlet cascade shows higher losses, which may be due to a separated region near the trailing edge. The contracting inlet cascade shows a noticeably lower loss from the top of the secondary loss core to the endwall. The inlet contraction is expected to reduce the strength of horseshoe vortex system and the resulting separation. The contraction also accelerates the inlet flow into the turbine passageway which may extend the laminar flow region on the endwall. Finally, the aft loaded vane, which locates the minimum pressure on the vane further along the passage may move the location where the passage vortex lifts the secondary loss core closer to the trailing edge. The aero-combustor comparison shows a similar but opposite effect. Generally, the two high turbulence loss curves show much higher profile losses than low turbulence cases due to early suction surface transition and higher levels of skin friction augmentation on the vane surface. Also, the high level of turbulence is expected to redistribute the flow across the span of the passage. Generally, the profile losses are quite similar midspan but the contracting inlet with its higher inlet turbulence level shows increased losses across the remainder of the passage. Two factors are suggested to be responsible for this result. Firstly, the high turbulence is expected to significantly reduce any disadvantage of the constant height inlet cascade due to the improved performance of flows with high turbulence in adverse pressure gradient regions. Secondly, the higher turbulence of contracting inlet cascade, due to its proximity to the combustor, can be expected to increase losses and mix away most identifiable features of the flow.

The cross-passage averaged loss for the contracting inlet cascade is presented for both the low and aero-combustor turbulence conditions across the three chord exit Reynolds numbers in **Figure 12**. The low turbulence case, shown with open symbols shows the most distinct variation with Reynolds number. The spanwise loss distributions show that the size of the secondary loss increases with decreasing Reynolds number while the position of the secondary loss core is convected further off the endwall. In the midspan region, the profile losses are shown to be two-dimensional and very similar in level. The cross passage losses for the aero-combustor turbulence case are much larger than the low turbulence cases across the entire span and are qualitatively very similar in nature. The lowest turbulence level case shows a noticeably higher level of total pressure loss across the span while the two higher Reynolds numbers are very similar in their level of losses.

Figure 13 presents the cross-passage averaged turning (β) as a function of span for the constant and contracting inlet cascades for the two turbulence conditions. The figure clearly shows the that aft loaded vane produces a noticeably increased turning angle. Qualitatively, the shape of the two low-turbulence turning-angle distributions are quite similar. However, the level of underturning is noticeably reduced for the contracting inlet cascade. The comparison between the two aero-combustor turning angle distributions is more pronounced. The contracting inlet cascade turning distribution appears to have no underturning across the entire profile. **Figure 14** presents the cross-passage averaged turning angle (β) for both the low and aero-combustor turbulence conditions across the three chord exit Reynolds numbers for the contracting inlet cascade. The turning angle for the low turbulence case is very similar for the three Reynolds numbers. However, the location and level of the underturning extends further off the endwall with decreasing Reynolds number. The aero-combustor turbulence is also qualitatively similar for the three Reynolds numbers but shows increased turning for increasing Reynolds numbers. Additionally, there appears to be a complete lack of underturning for this contracting inlet cascade at the high turbulence condition.

Passage Averaged Loss Comparison. Passage averaged losses are presented in **Figure 15** comparing the two cascades as a function of exit chord Reynolds numbers for the low and aero-combustor turbulence conditions. The comparison between the constant height and contracting inlet cascades paint a promising picture for the inlet contraction in terms of loss reduction. The contracting inlet cascade reduces the average fractional total pressure loss by 0.0068 or 0.68%. Considering the maximum loss is 0.0468 or 4.68% this reduction is very significant. This reduction in losses is attributed to a reduction in the strength of the horseshoe vortex system due to the flow acceleration near the stagnation region. Additionally, the contraction is expected to move transition further downstream in the turbine passage. The inlet contraction appears to have the opposite influence on losses for the aero-combustor turbulence. The two lowest Reynolds numbers show an increase in losses of 0.0035 or 0.35% while the highest Reynolds number shows a increased loss of over .011 or 1.1%. This large increase in loss is attributed to the more aggressive turbulence encountered by the contracting inlet cascade. The integration of the cascade into the combustor exit nozzle effectively moves the cascade 32 cm closer to the aero-combustor simulator, significantly raising the level of the turbulent kinetic energy. This higher turbulence is expected to promote earlier transition and further enhance the augmentation of skin friction. Generally, turbulence has been found to reduce endwall losses [7], eliminating much of the beneficial influence of the contracting inlet.

SUMMARY AND CONCLUSIONS

The present investigation compared exit losses for two vane cascades, one with a constant height inlet and one with a contracting

inlet. The exit surveys were acquired at two turbulence levels, low and aero-combustor, across a four to one range (500,000, 1,000,000, and 2,000,000) in exit chord Reynolds number. The low turbulence data for the constant inlet height cascade showed a thin two-dimensional wake near midspan due to the laminar boundary layers developing on the vane surfaces. The low turbulence loss contours exhibited a significant secondary loss core that had been convected well off the endwall. A noticeable corner vortex and mild over turning near the endwall were also present. The main difference noted due to the contracting inlet cascade was reduced circumferentially averaged losses in the first quarter of span and reduced convection of the secondary loss core off the endwall. Additionally, the contracting inlet cascade at the low turbulence condition exhibited a substantially reduced (0.7%) passage averaged total pressure loss compared with the constant inlet height cascade. The turning angle also exhibited less under turning than the constant inlet height cascade. The constant height cascade used a fully loaded vane profile while the contracting inlet cascade used an aft loaded vane profile. At the low turbulence condition, the aft loaded vane appeared to produce slightly lower profile losses compared with the fully loaded vane. However, this difference was on the order of the measurement uncertainty. At the aero-combustor turbulence condition the losses for the constant height inlet cascade displayed much broader wakes with little time averaged evidence of a discrete secondary loss core. The aero-combustor case also showed strong evidence of a corner vortex in addition to a significant level of over turning near the endwall. The contracting inlet height had qualitatively similar results. However, the measured passage averaged loss for the contracting inlet cascade was significantly higher compared with the constant inlet cascade. At high inlet turbulence, the expected benefit for the contracting inlet over the constant height inlet is expected to be significantly reduced. Also, the contracting inlet effectively moved the leading edge plane of the cascade into the exit of the mock combustor where the turbulence condition was much more aggressive. This more aggressive turbulence is believed to have caused additional skin friction and mixing losses within the cascade.

ACKNOWLEDGEMENTS

The authors would like to gratefully acknowledge the support from the University of North Dakota for the graduate students who conducted this work. The authors would also like to acknowledge the prior support from the Advanced Gas Turbine System Research (AGTSR) consortium, largely funded by DOE's National Energy Technology Laboratory for the fabrication of the cascade test sections. The facility used in this project was funded with a seed grant from the North Dakota EPSCoR Program. In addition, the authors are indebted to the University of North Dakota for providing additional support and laboratory space.

REFERENCES

[1] Ames, F.E., Wang, C., and Barbot, P.A., 2003, "Measurement and prediction of the influence of catalytic and dry low NOx Combustor Turbulence on Vane Surface Heat Transfer," J. Turbomachinery, vol. 125, pp. 210-220.

[2] Ames, F.E., Argenziano, M., Wang, C., 2004, "Measurement and Prediction of Heat Transfer Distributions on an Aft Loaded Vane Subjected to the Influence of Catalytic and Dry Low NOx Combustor Turbulence," J. Turbomachinery, vol 126, pp. 139-149.

[3] Ames, F.E., Barbot, P.A., Wang, C., 2003, "Effects of Aeroderivative Combustor Turbulence on Endwall Heat Transfer Distributions Acquired in a Linear Vane Cascade," ASME Journal of Turbomachinery, vol. 125, pp. 221-231.

[4] Denton, J.D., 1993, "Loss Mechanisms in Turbomachines," J. of Turbomachinery," vol. 115, pp. 621-656.

[5] Glassman, A.G., ed, 1972-1975, "Turbine Design and Application," Vols. 1-3, NASA SP-290.

[6] Moore, J., Shaffer, D.M., and Moor, J.G., 1987, "Reynolds Stress and Dissipation Downstream of a Turbine Cascade," J. Turbomachinery, vol. 109. pp. 258-267.

[7] Gregory-Smith, D.G., and Cleak, J.G.E., 1992, "Secondary Flow Measurements in a Turbine Cascade with High Inlet Turbulence," J. of Turbomachinery, vol. 114. pp. 173-183.

[8] Ames, F.E. and Plesniak, M.W., 1997, "The Influence of Large Scale, High Intensity Turbulence on Vane Aerodynamic Losses, Wake Growth, and Exit Turbulence Parameters," J. Turbomachinery, vol. 119, pp. 182-192.

[9] Sieverding, C.H., 1985, "Recent progress in the understanding of basic aspects of secondary flow in turbine blade passages," J. Engineering for Gas Turbines and Power, vol. 107, pp. 248-257.

[10] Klein, A., 1966, "Investigation of the entry boundary layer on the secondary flows in the blading of axial turbines, BHRA T 1004.

[11] Langston, L.S., Nice, M.L., and Hooper, R.M., 1977, "Three dimensional flow within a turbine cascade passage," J. Engineering for Power, January, 1977, pp. 21-28.

[12] Marchal, P., and Sieverding, C.H., 1977, "Secondary flows within turbomachinery bladings," Secondary Flows in Turbomachines, AGARD CP 214.

[13] Burd, S.W., and Simon, T.W., "Flow measurements in a nozzle guide vane passage with a low aspect ratio and endwall contouring," J. Turbomachinery, Vol. 122, pp. 659-666.

[14] Zess, G.A. and Thole, K.A., 2001, "Computational design and experimental evaluation of using an inlet fillet on a gas turbine vane," ASME Paper No. 2001-GT-404.

[15] Becz, S., Majewski, M.S., and Langston, L.S., 2003, "Leading edge modification effects on turbine cascade endwall loss," ASME Paper No. GT2003-38898.

[16] Becz, S., Majewski, M.S., and Langston, L.S., 2004, "An experimental investigation of contoured leading edges for secondary flow loss reduction," ASME Paper No. GT2004-53964.

[17] Ingram, G., Gregory-Smith, D., Rose, M., Harvey, N., and Brennan, G., 2002, "The effect of end-wall profiling on secondary flow and low development in a turbine cascade," ASME Paper No. GT2002-30339.

[18] FLUENT 6.0, 2001, FLUENT 6.0 User's Guide, Fluent, Inc., Lebanon, N.H.

[19] Moffat, R.J., 1988, "Describing the uncertainties in experimental results," Experimental Thermal and Fluid Science, vol. 1., pp. 3-17.

[20] Ames, F. E., Johnson, J. D., and Fiala, N. J., 2006, "The Influence of Aero-Derivative Combustor Turbulence and Reynolds number on Vane Aerodynamic Losses, Secondary Flows, and Wake Growth," ASME Paper No. GT2006-90168.

Vane Geometries	Aff Loaded	Front Loaded
True Chord (cm)	47.35	47.78
Axial Chord (cm)	25.40	25.00
Scale	11	11
Leading Edge Dia. (cm)	5.35	5.59
Trailing Edge Dia. (cm)	0.98	0.98
Stagger Angle	56.8°	55.1°
Calc. Exit Angle	74.4°	73.98°

Table 1. Comparison of aft and forward loaded vane geometries

Flat Endwall	Reynolds	Tu	U (m/s)	Lx (cm)	Lu (cm)	ε (m^2/s^3)
low turbulence [LT]	500,000	0.0069	4.96	8.12	127.0	0.00005
	1,000,000	0.0076	10.43	5.02	154.5	0.00035
	2,000,000	0.0060	18.71	3.58	15.5	0.0144
aero-derivative combustor [AC]	500,000	0.1313	5.24	3.68	7.24	6.67
	1,000,000	0.1402	9.32	3.52	6.36	51.5
	2,000,000	0.1339	18.39	3.58	7.35	302.0
Contoured EW	Reynolds	Tu	U (m/s)	Lx(cm)	Lu(cm)	ε(m^2/s^3)
low turbulence	500000	0.0083	3.61	5.72	24.4	0.0001
[LT]	1000000	0.0132	7.74	0.75	134.5	0.0012
	2000000	0.0086	14.83	6.90	21.38	0.0143
aero-derivative	500000	0.2091	4.46	4.41	6.11	19.95
combustor	1000000	0.2113	8.31	4.37	6.30	128.90
[AC]	2000000	0.2032	16.98	4.48	7.22	853.8

Table 2. Inlet turbulence characteristics for flat and contracting inlet cascade tests

Flat Endwall	Low Turbulence			Aero-Combustor		
$Re_{C,EX}$	504,625	1,020,404	1,950,421	498,411	994,597	1,945,690
$T_{T,IN}$ (K)	300.48	297.82	310.95	302.86	301.58	308.80
$P_{T,IN}$ (Pa)	99,162	101,387	100,231	99,133	99,252	98,802
V_{EX} (m/s)	17.01	33.36	71.98	17.04	33.97	71.17
Ma_{EX}	0.0489	0.0964	0.2028	0.0488	0.0975	0.2012
Ω (Full)	0.0456	0.0366	0.0357	0.0635	0.0567	0.0492
Ω (Midline)	0.0458	0.0240	0.0216	0.0489	0.0477	0.0405
β (Full)	73.23	73.59	73.63	73.15	73.67	73.76
β (Midline)	73.13	74.14	74.13	72.77	73.52	73.68
Contracting	Low Turbulence			Aero-Combustor		
$Re_{C,EX}$	499,776	972,865	1,992,349	505,766	980,139	1,952,438
$T_{T,IN}$ (K)	300.23	299.47	301.55	294.94	297.43	305.08
$P_{T,IN}$ (Pa)	98,255	99,040	98,729	98,564	98,914	98,817
V_{EX} (m/s)	17.14	33.19	71.43	16.60	32.76	70.61
Ma_{EX}	0.0493	0.0956	0.2043	0.0482	0.0947	0.2009
Ω (Full)	0.0368	0.0311	0.0295	0.0672	0.0600	0.0604
Ω (Midline)	0.0239	0.0188	0.0200	0.0501	0.0462	0.0469
β (Full)	75.04	75.28	75.45	75.08	75.39	75.53
β (Midline)	75.57	75.61	75.57	73.85	74.54	74.77

Table 3. Conditions, mass averaged loss and turning angle for conventional and contracting inlet cascade at low (LT) and aero-combustor (AC) turbulence, ¼ axial chord.

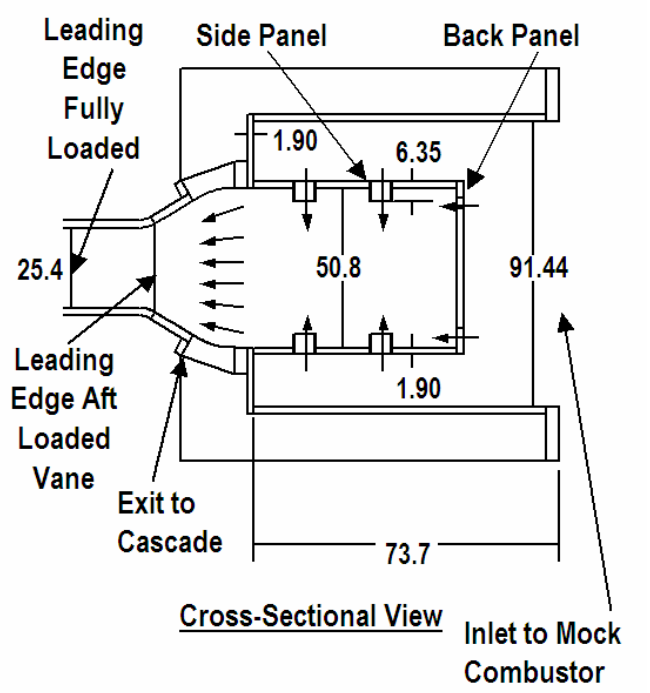

Figure 1. Schematic of mock combustor turbulence generator in aero-derivative configuration showing interface with cascade.

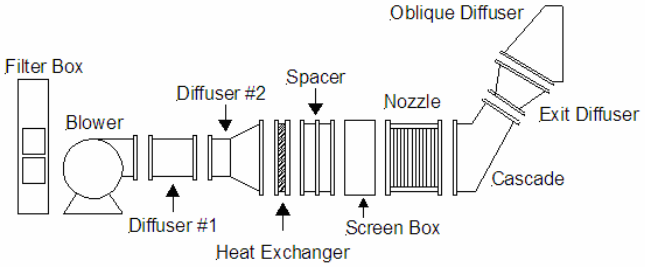

Figure 2. Large scale low speed cascade facility.

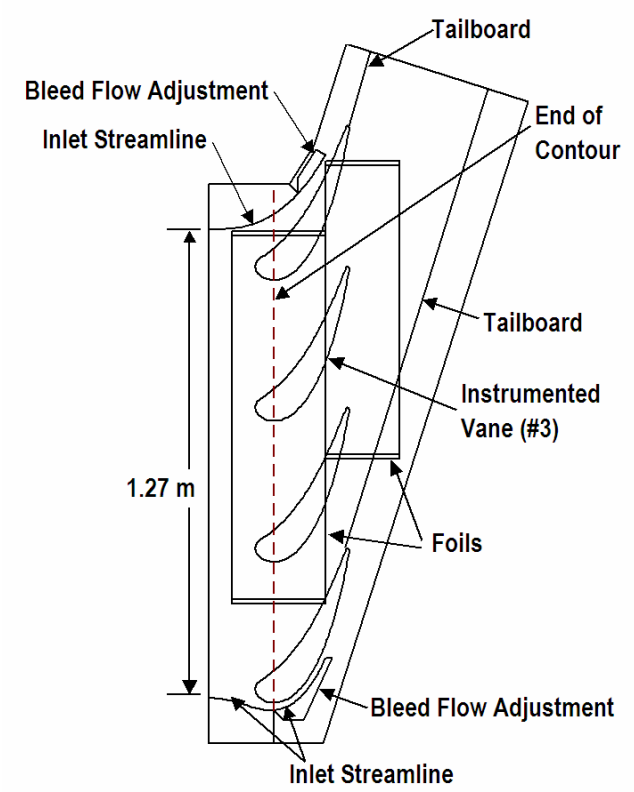

Figure 3. Schematic of contracting endwall cascade facility.

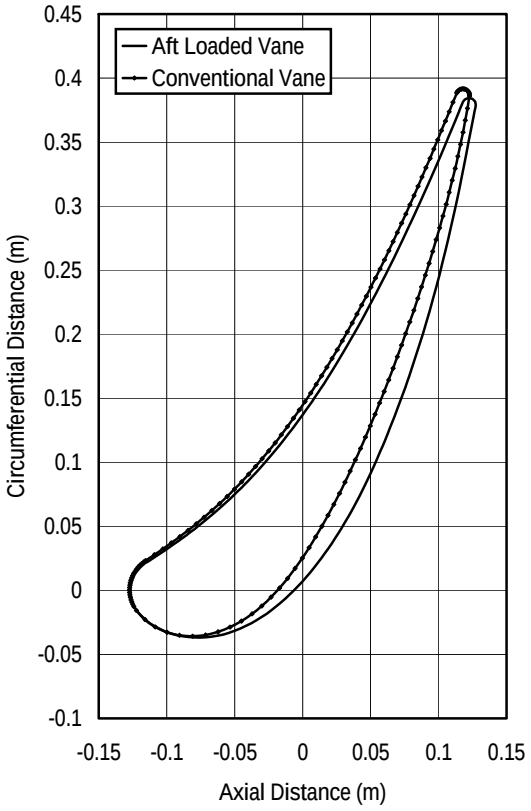

Figure 4. Comparison between conventional and aft loaded vane.

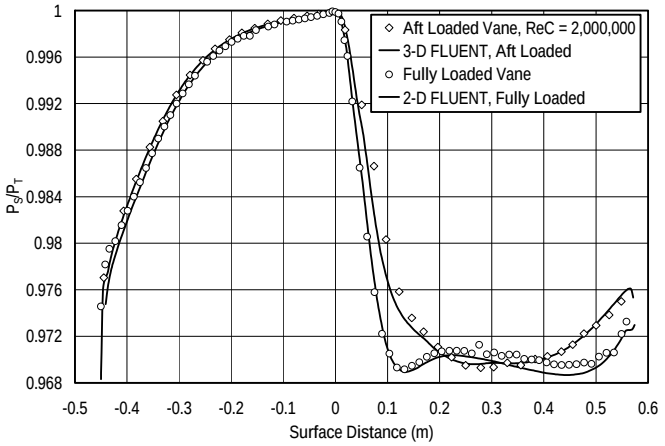

Figure. 5 Comparison between measured and predicted vane midspan pressure distributions for aft and fully loaded vanes.

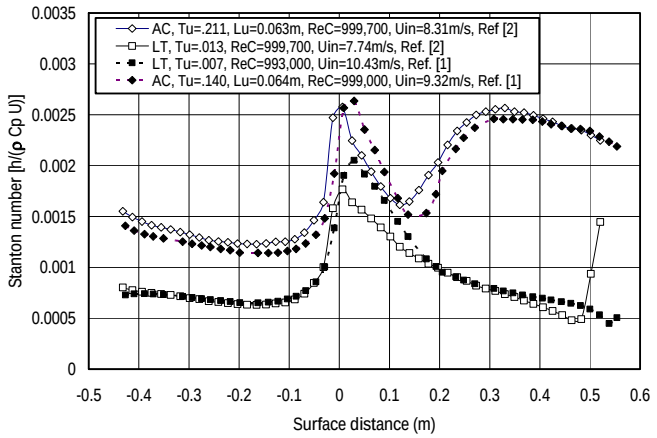

Figure 6. Comparison between conventional and aft loaded vane heat transfer distributions, Re_C = 1,000,000, low and aero-combustor turbulence.

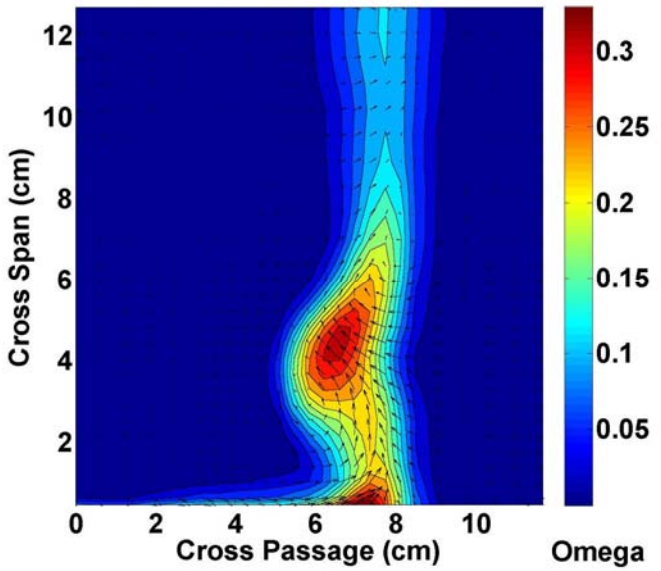

Figure 7. Total pressure loss contours with secondary velocity vectors for conventional cascade for low turbulence condition, Reynolds No. = 1,000,000.

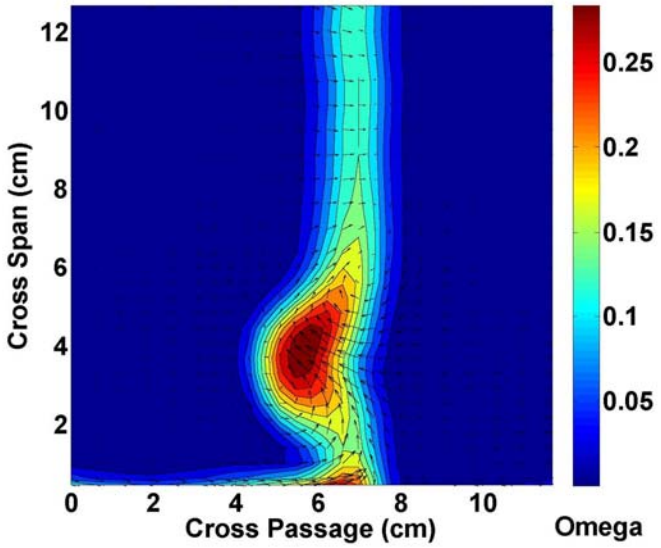

Figure 8. Total pressure loss contours with secondary velocity vectors for contracting inlet cascade for low turbulence condition, Reynolds No. = 1,000,000.

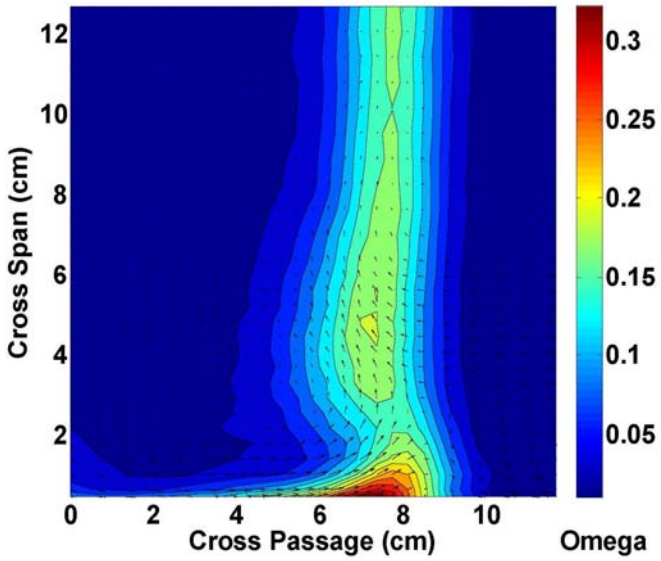

Figure 9. Total pressure loss contours with secondary velocity vectors for conventional cascade for aero-combustor turbulence condition, Reynolds No. = 1,000,000.

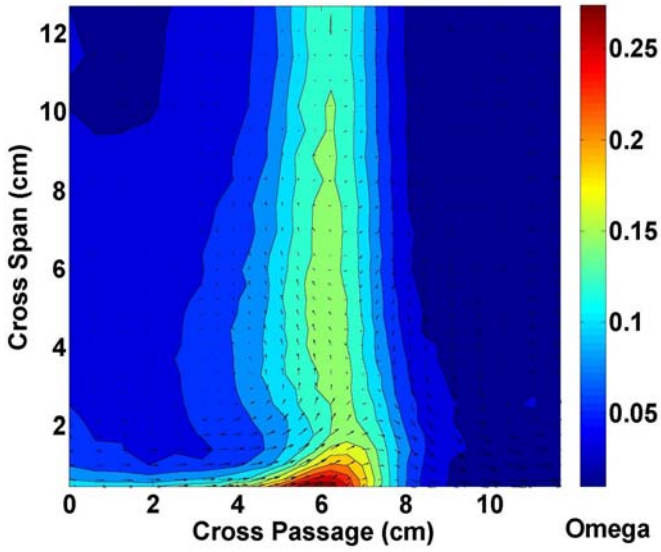

Figure 10. Total pressure loss contours with secondary velocity vectors for contracting inlet cascade for low turbulence condition, Reynolds No. = 1,000,000.

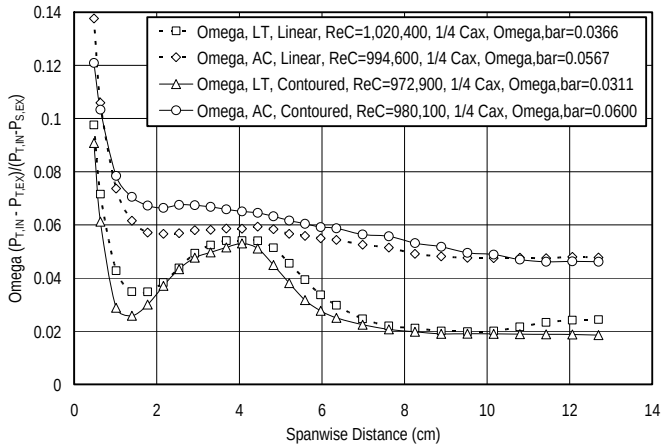

Figure 11. Cross passage averaged total pressure loss (Ω) versus span comparing turbulence condition and cascade geometry effects, Re_C = 1,000,000.

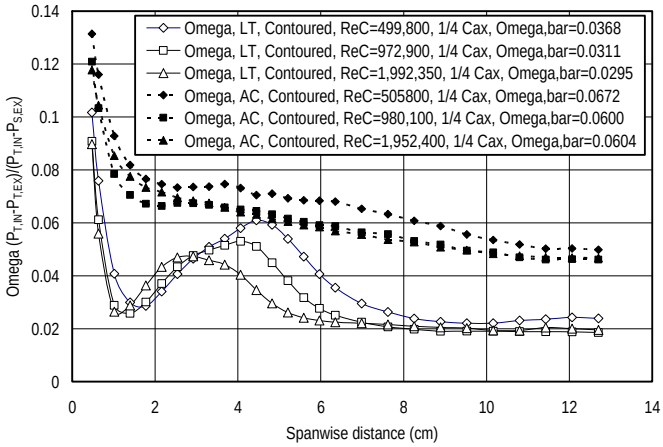

Figure 12. Cross passage averaged total pressure loss (Ω) versus span for contracting inlet cascade comparing turbulence condition and Reynolds number effects.

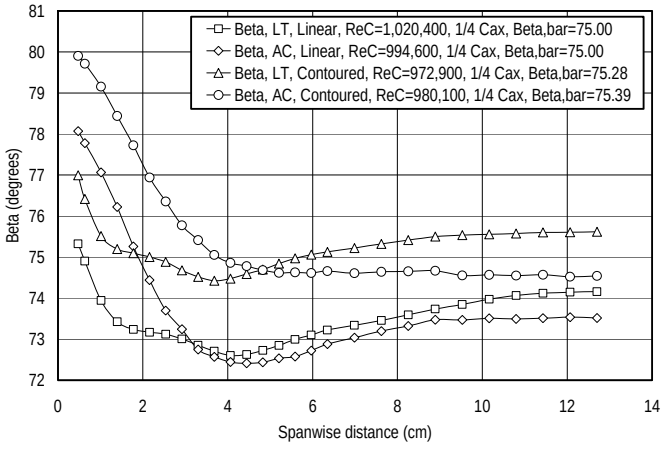

Figure 13. Cross passage averaged turning angle (β) versus span comparing turbulence condition and cascade geometry effects, Re_C = 1,000,000.

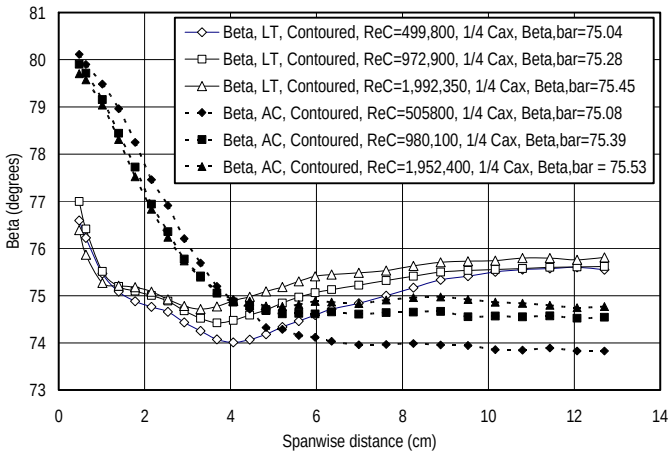

Figure 14. Cross passage averaged turning angle (β) versus span for contracting inlet cascade comparing turbulence condition and Reynolds number effects.

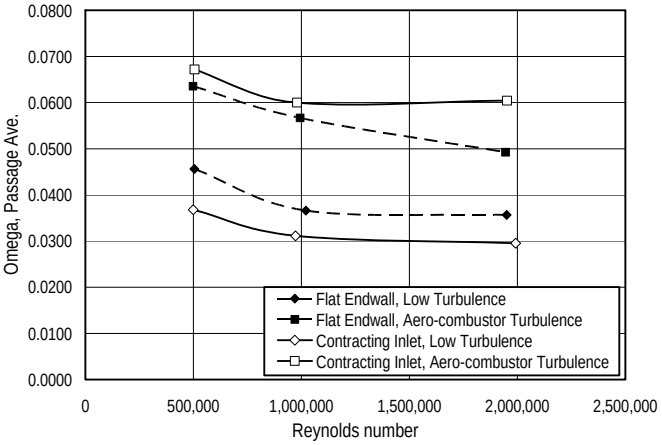

Figure 15. Comparison of passage averaged losses comparing flat with contracting inlet cascade at low and aero-combustor turbulence, Re_C = 500,000, 1,000,000, and 2,000,000.